#### FIELD REPORT



WILEY

# Field observation of tornadic supercells by multiple autonomous fixed-wing unmanned aircraft

Eric W. Frew<sup>1</sup> | Brian Argrow<sup>1</sup> | Steve Borenstein<sup>1</sup> | Sara Swenson<sup>1</sup> | C. Alexander Hirst<sup>1</sup> | Henno Havenga<sup>2</sup> | Adam Houston<sup>3</sup>

#### Correspondence

Eric W. Frew, Ann and H.J. Smead Department of Aerospace Engineering Sciences, University of Colorado Boulder, Boulder, CO 80309. Email: eric.frew@colorado.edu

#### **Abstract**

This paper presents the results of the design and field deployment of multiple autonomous fixed-wing unmanned aircraft into supercell thunderstorms. As part of a field campaign in Spring 2019, up to three fixed-wing unmanned aircraft were deployed simultaneously into different regions of supercell thunderstorms, To learn more about the atmospheric conditions that lead to the formation of tornadoes. Successful field deployment is attributed to (a) a nomadic concept of operations that allows the unmanned aircraft system team and science team to work seamlessly together while satisfying all aviation regulations and (b) the ruggedized RAAVEN unmanned aircraft system with modular features that favor rapid, ease-of-use over the brute strength of previous designs. The concept of operations and the unmanned aircraft system are described along with results from a 4 day window where four storms were sampled: two of these storms were tornadic (formed tornadoes before, during, or after being sampled) and two were not. These results validate the feasibility of nomadic operation of multiple unmanned aircraft simultaneously in severe weather conditions. Further, the successful field deployments demonstrate the importance of the modular unmanned aircraft design.

#### **KEYWORDS**

autonomy, drones, environmental monitoring, multi-robot, severe weather, supercell thunderstorms, unmanned aircraft systems

# 1 | INTRODUCTION

The study of severe local storms is well-suited for unmanned aircraft systems since the spatial and temporal domains can be relatively short and flying piloted aircraft into these environments is too dangerous. The rapid growth of unmanned aircraft system (UAS) technology and open source avionics has enabled various academic and government institutions to deploy UAS for atmospheric science (Bonin, Chilson, Zielke, & Fedorovich, 2012; Curry, Maslanik, Holland, & Pinto, 2004; Dias, Gonçalves, Freire, Hasegawa, & Malheiros, 2012; Elston, Roadman, et al., 2011; Frew, Elston, Argrow, Houston, & Rasmussen, 2012; Holland et al., 2001; Jacob, Chilson, Houston, & Smith, 2018; Lin & Lee, 2008; Reuder,

Brisset, Jonassen, Müller, & Mayer, 2009; van den Kroonenberg, Martin, Beyrich, & Bange, 2012). However, only a handful of efforts have attempted to fly aircraft (piloted or unmanned) into supercell thunderstorms, the type of storm known to produce the most violent tornadoes (Lemon & Doswell, 1979). A piloted T-28 aircraft was used to penetrate hailstorms (some supercells) at midlevels to measure hail (Sand, 1976). Another piloted aircraft (Electra) was used in the first Verification of the Origins of Rotation in Tornadoes Experiment (VORTEX) to make radar observations from ahead of the storm. Neither case flew near to the ground in the important rear-flank downdraft region (Lemon & Doswell, 1979). The Tempest UAS was the first unmanned aircraft system designed specifically for sampling severe storms

<sup>&</sup>lt;sup>1</sup>Ann and H.J. Smead Department of Aerospace Engineering Sciences, University of Colorado Boulder, Boulder, Colorado

<sup>&</sup>lt;sup>2</sup>Faculty of Natural and Agricultural Sciences, North West University, Potchefstroom, South Africa

<sup>&</sup>lt;sup>3</sup>Department of Earth and Atmospheric Sciences, University of Nebraska, Lincoln, Nebraska





**FIGURE 1** The left image shows a tornado formed from one of the supercell thunderstorms being sampled by a RAAVEN unmanned aircraft system on May 17, 2019. The right image shows the supercell thunderstorm sampled on May 18, 2019 [Color figure can be viewed at wileyonlinelibrary.com]

(Elston, Argrow, Frew, Houston, & Straka, 2011; Roadman, Elston, Argrow, & Frew, 2012) and was deployed during the second Verification of the Origins of Rotation in Tornadoes Experiment 2 (VORTEX2; VORTEX2, 2008) where it performed the first ever sampling of the rear-flank gust front of a supercell thunderstorm (Elston, Roadman, et al., 2011). Those deployments are the only reported flights of an unmanned aircraft into supercell thunderstorms.

This paper describes the hardware and software platform, autonomous concept of operations, and results of field deployment of multiple autonomous unmanned aircraft simultaneously to study tornado formation in supercell thunderstorms (Figure 1) as part of the Targeted Observation by Radars and UAS of Supercells (TORUS) project (TORUS, 2019). The TORUS project <sup>1</sup> is conducted by more than 50 scientists and students deploying a broad suite of cutting-edge instrumentation into the US Great Plains during the 2019 and 2020 storm seasons. Led by the University of Nebraska-Lincoln, TORUS also involves the University of Colorado Boulder, Texas Tech University, the NOAA National Severe Storms Laboratory, and the Cooperative Institute for Mesoscale Meteorological Studies. TORUS instrumentation includes four unmanned aircraft systems (drones), three mobile radars, eight mobile mesonets (trucks mounted with meteorological instrumentation), a mobile LIDAR (similar to a radar but using an eye-safe laser), three mobile sounding systems (balloon-borne sensor packages), and the NOAA P3 manned aircraft (TORUS, 2019).

TORUS aims to use the data collected to improve the conceptual model of supercell thunderstorms (the parent storms of the most destructive tornadoes) by exposing how small-scale structures such as rear-flank internal surges and associated boundaries (Kosiba et al., 2013; Skinner et al., 2014), left-flank convergence boundaries (Beck & Weiss, 2013), left-flank vertical vorticity sheets (Orf, Wilhelmson, Lee, Finley, & Houston, 2017; Snyder, Bluestein, Venkatesh, & Frasier, 2013),

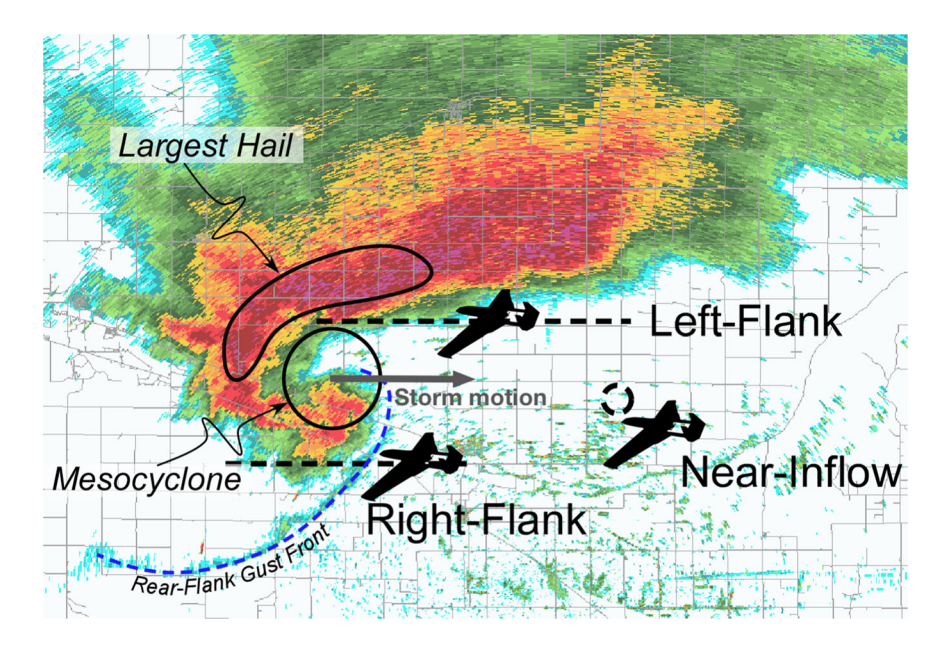
and the streamwise vorticity current (Orf et al., 2017) within these storms might lead to tornado formation. Evidence from prior research (Dahl, Parker, & Wicker, 2012; Kosiba et al., 2013; Orf et al., 2017; Skinner et al., 2014) supports the hypothesis that the source and amplification of circulating air that leads to tornadogenesis depend upon these small-scale structures.

In addition to the description of the unmanned aircraft system and concept of operations, the results of deployments over a 4 day window are presented. These are the first 4 days of the TORUS 2019 field campaign where the TORUS team intercepts and samples four different supercell thunderstorms. A video compiled from operations throughout the TORUS campaign, with footage from onboard the aircraft, is included in the online version of this article. This paper focuses specifically on the unmanned aircraft system and its performance, and not on the scientific hypothesis being tested or the coordination and output of all TORUS instruments. That discussion is left to future publications. Unlike the VORTEX2 field campaign (Elston, Roadman, et al., 2011) where only a single unmanned aircraft was deployed in the relatively benign rear flank region that typically does not experience much precipitation, this study describes the coordinated deployment of up to three unmanned aircraft simultaneously in different regions of the storm, including the high-risk forward flank that is in the direct path of the heaviest precipitation. Lessons learned are presented on the design of unmanned aircraft systems and deployment strategies for sampling supercell thunderstorms and other similar severe local storms.

# 2 | CONCEPT OF OPERATIONS

The concept of operations developed for sampling supercell thunderstorms in driven by the location of the three regions that need to be sampled and by federal aviation regulations. Since this paper focuses on the unmanned aircraft system and its performance, the scientific hypothesis that make the regions important is not

FIGURE 2 The TORUS operations plan has three different unmanned aircraft system teams: left flank, right flank, and near inflow. These areas are defined relative to a typical radar reflectivity image of a supercell thunderstorm with typical west to east storm motion indicated. Here the colored shading represents the density of precipitation (rain and hail). The main areas of the supecell are identified (mesocyclone, hail core, and rear-flank gust front). The dashed lines indicate the nominal flight path of each aircraft in different areas [Color figure can be viewed at wileyonlinelibrary.com]



discussed and can be found in Dahl et al. (2012), Kosiba et al. (2013), Orf et al., (2017), and Skinner et al. (2014). From a scientific standpoint, it is sufficient to state that the goal is to fly in the three regions described below simultaneously while the other TORUS instruments (TORUS, 2019) are also measuring the storm.

#### 2.1 | Storm regions

Data collection by the UAS is focused in three locations defined relative to storm motion and the mesocyclone. A typical supercell thunderstorm moves east or northeast (left to right in Figure 2) with bulk storm speed of 20–40 m/s. The three storm-relative locations are: the "left-flank" (LF), located left of the mesocyclone (when facing the direction of storm motion); the "right flank" (RF); and "near inflow" (NI), located 10 km in front of the supercell (Figure 2).

The *left flank team* <sup>2</sup> is primarily focused on data collection in the region left (typically north) of the mesocyclone and principal storm updraft and on the upstream (usually eastern) margins of the largest hail (Figure 2). A typical mission starts 15–30 km in front of the storm, and travels toward the storm. Once close to the precipitation in the center of the storm, the aircraft turns around and travels downstream (relative to storm motion). If storm motion is slow enough and the road network supportive, additional transects into and out of the storm are executed. This mission is the most dangerous and complex of the three because it travels closest to the hail core (Largest Hail region of Figure 2), and if the aircraft slows or has to stop the storm can overtake the aircraft. To land the aircraft, the left flank mission must outrun the storm a sufficient distance. This motivates the need for a system that can be landed and stowed quickly.

The *right flank team* is typically south of the mesocyclone and principal storm updraft (Figure 2). This mission aims to sample the rear flank gust front (Lemon & Doswell, 1979) that delineates inflow/ambient air from rear-flank outflow. Similar to the left flank mission, the right flank mission starts in advance of the storm. It continues into the storm and past the gust front 5–7 km into the outflow. The aircraft turns around and completes additional passes across the front as time allows. Unlike the left flank mission, the right flank mission is not directly in the path of the largest hail but can still encounter heavy rain, small hail, and strong winds associated with downbursts within the outflow.

The *near inflow team* conducts stationary profiles (orbits about a fixed location at a fixed height and/or constant ascent and descent rates) on inflow/ambient air ahead of the supercell (Figure 2). In contrast to the aircraft in the left flank and right flank, the aircraft flying in the near inflow does not conduct mobile data collection via *Follow Me*. Once the near inflow aircraft is launched it will typically loiter in a set area at various altitudes. The near inflow mission can last from 10 min to over an hour and terminates operations once the storm or the associated lightning get too close.

### 2.2 | Regulatory requirements

All flights conducted during the TORUS campaign are in full compliance with Federal Aviation Administration regulatory requirements. The flights are conducted under multiple Certificates of Waiver or Authorization (COAs; FAA, 2008). As a public university, the University of Colorado Boulder is able to fly under a COA as opposed to the Part 107 Small UAS regulations (FAA, 2019) used by commercial entities. In addition to defining flight boundaries, the COA allows the University of Colorado Boulder to certify its pilots and to certify the airworthiness of its UAS.

Several main requirements drive the concept of operations described below. First, the COAs limit the altitude at which the aircraft can fly.

<sup>&</sup>lt;sup>2</sup>Italics are used the first time critical terms are defined that are used verbatim in the field. For example, during operations the team often refers to the "left flank aircraft" when coordinating flights.

These limits vary by geographical region, with the COAs allowing flight up to 2500 ft above ground level in most locations. Second, the COAs require that the aircraft is in visual line of sight of a visual observer (VO) at all times. This line of sight requirement is defined to mean the aircraft must be within 0.5 miles laterally of the Visual Observer at all times. Third, the aircraft can only operate in visual meteorological conditions in which visual flight rules are followed. This essentially means the aircraft must stay 500 meters below the clouds at all times. Finally, the aircraft can operate until 30 min after sunset, which is approximately 21:00 Central Daylight Time in the flight domain.

# 2.3 | Airspace management

Airspace management for these operations is conducted by a team that includes all *pilots in command (PICs)* and an additional flight coordinator. The COAs specify that each aircraft has its own pilot in command whereas the flight coordinator role is added by our team. Because the region of operations for the field campaign is so large, the UAS operate in airspaces with a large variety of conditions or constraints. For example, some airports require advance notice 4 hr before operations nearby while others only require being on a local aviation radio channel. To ensure full compliance, each UAS PIC coordinates its operation with the flight coordinator. Before launch the team of pilots and flight coordinator study the expected flight areas and make the required advanced notifications. During flight operations the flight coordinator maintains situational awareness of the entire UAS team while the individual PICs focuses on their aircraft and other flight traffic in their local area only.

#### 2.4 | Follow me

To satisfy the COA requirements while performing atmospheric sampling over 10-100 mile transects, a multivehicle concept of operations was developed where the aircraft follows a ground vehicle that carries the pilot in command and visual observer. In particular, a nomadic Follow Me capability is achieved using three ground vehicles (Elston, Roadman, et al., 2011). A Tracker vehicle carries the pilot in command and the visual observer and additional operator interfaces for the aircraft. The position and velocity of the Tracker is determined from GPS and the aircraft is commanded to follow the Tracker with adjustable cross-track and alongtrack offsets. The Tracker follows a Combined Mesonet and Tracker (CoMeT; Hanft & Houston, 2018) that is led by the meteorologists including the mission lead. This vehicle measures the atmospheric state in the near-surface layer to compare with the readings from the aircraft. Finally, a Scout vehicle drives 1-2 miles ahead of the Tracker and CoMeT to report road conditions as well as precipitation so the aircraft can avoid heavy rain and hail.

# 2.5 | Stack

While the standard mission has aircraft operating in different parts of the storm (Section 2.1), when road networks are limited multiple aircraft are flown in a loosely coordinated *stack* formation. Here, two different aircraft are assigned to different Trackers at different altitudes, and they both follow a single lead CoMeT.

# 3 | RAAVEN UNMANNED AIRCRAFT SYSTEM

The Robust Autonomous Aerial Vehicle—Endurant and Nimble (RAAVEN) unmanned aircraft system was designed and built by the University of Colorado Boulder Integrated Remote and In Situ Sensing (IRISS)<sup>3</sup> team, with collaboration from Rite-Wing RC on the design and manufacture of the ruggedized, long-endurance airframe. The success of RAAVEN for severe storm sampling is attributed to a comprehensive custom-designed system described here.

#### 3.1 | Airframe

The RAAVEN airframe (Figures 3 and 4) fuselage is molded from a very durable EPP foam used for the automotive industry, and the wings and tail are custom cut, lightened, and skinned at Rite-Wing RC in Mesa, AZ. The result is an extremely robust and rigid airframe. The aircraft weighs 6.8 kg, including over 600 Wh of Li-ion battery cells, and has a wingspan of 2.3 m. At a cruise speed of 17 m/s, the aircraft has 3 hr of endurance.

#### 3.2 | Avionics

Avionics and telemetry are based on the open-source ArduPilot firmware <sup>4</sup> and hardware and COTS radio systems by MicroHard, built into a custom PCB. A Teensy microcontroller relays payload and telemetry data to the autopilot, whose MAVLINK communication protocol was modified to route these messages to the ground station.

#### 3.3 | Payload sensors

Primary meteorological payload sensors on the RAAVEN include: the Black Swift Technologies 3D multihole probe (MHP) which provides true air speed (TAS), angle of attack (AOA), and sideslip angle (AOS), the VectorNav VN-200 ruggedized, temperature calibrated inertial measurement unit (IMU), and the Vaisala RSS-421 pressure, temperature, and humidity (PTH) sonde. Redundant sensors include an additional IMU and iMet EE03 PTH sonde built into the Black Swift Technologies multihole probe, and GPS, attitude and derived winds from the autopilot. Data is logged at the output rate of each sensor on an onboard time-synchronized customized data logger, as well as

<sup>&</sup>lt;sup>3</sup>https://www.colorado.edu/iriss/

<sup>4</sup>http://ardupilot.org/

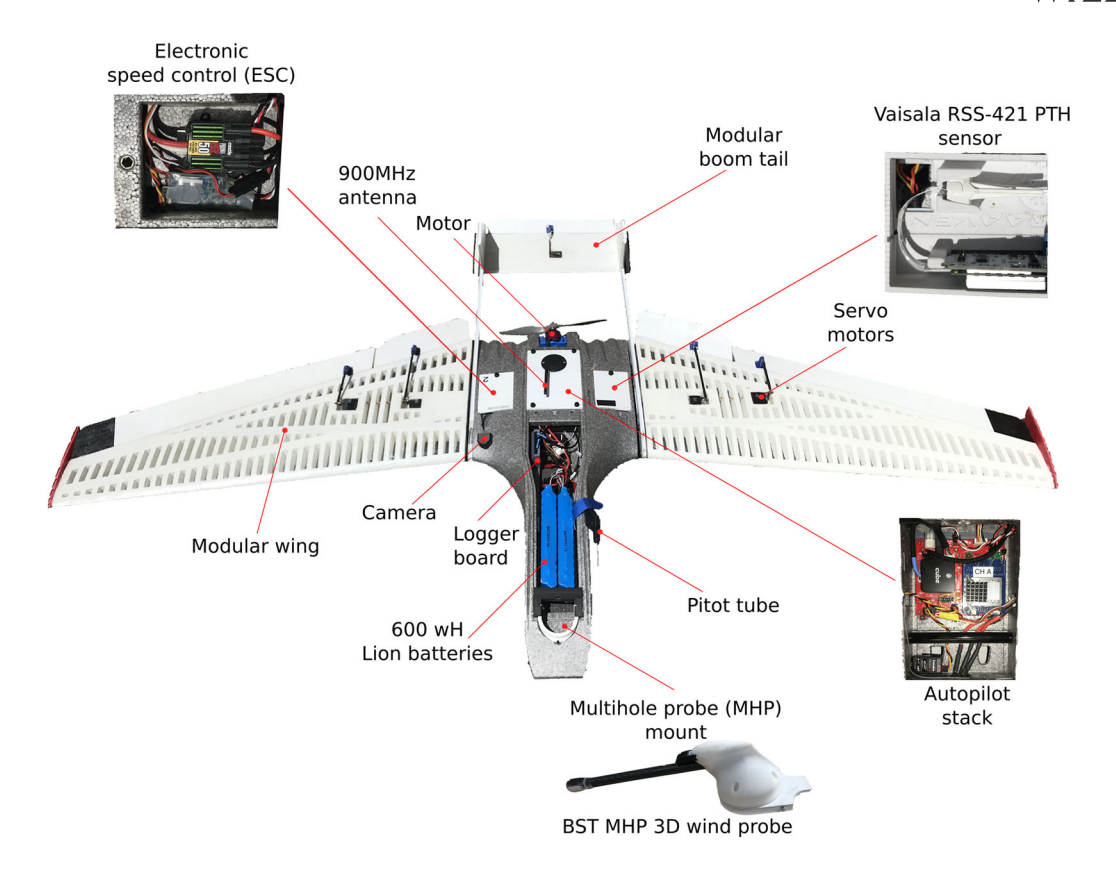


**FIGURE 3** The top view of the RAAVEN unmanned aircraft along with the main components of the airframe, the avionics, and the meteorological sensors [Color figure can be viewed at wileyonlinelibrary.com]

a low rate (1 Hz) telemetry stream in the ground station. Three-dimensional wind velocity is calculated from the multihole probe data and the aircraft state derived from the IMU (Nichols, Argrow, & Kingston, 2017). A small video camera is also mounted on the aircraft fuselage just before the root of the wing. The camera does not provide online atmospheric science data, but is useful to understand system behaviors after the flights.

# 3.4 | Launch and ground support

The Rapid Aircraft Pnuematic Catapult (RAPCat) enables the launching of aircraft in under 5 min from parking at a given location. The catapult is installed on the roof of the Tracker sport utility vehicle (Figure 4). The Tracker is also the mobile command center for the aircraft during flight operations.





**FIGURE 4** Left: The RAAVEN unmanned aircraft waiting for flight control systems to initialize. Right: Tracker 1 with the RAPCAT configured for launch. During nomadic operations, the RAAVEN undergoes preflight checks while sitting on the two posts extending from the back of the Tracker [Color figure can be viewed at wileyonlinelibrary.com]

#### 3.5 | Nomadic navigational controller

RAAVEN autonomy is provided by an architecture that combines onboard and ground-based algorithms to create the Follow Me capability (Figure 5). Onboard the aircraft, a supervisory computer interfaces between the autopilot and payload sensors, and autonomy software located on the Tracker vehicle. The supervisory computer relays the sensor data to the ground at 1 Hz while also sending it to an SD card on the data logger onboard at the raw sensor rate. Thus, in the event that an aircraft is damaged and the data logger is lost, atmospheric science data is still collected.

The heart of the autonomy architecture is the Nomadic Navigational Controller (NNC) which provides the control and operator interface for Follow Me operations. While the NNC provides similar tracking capability to the UAS fielded in the VORTEX2 campaign (Elston, Roadman, et al., 2011), the current hardware and software implementations are more complex and more robust. The NNC system and user interface was optimized for an operator in a moving vehicle to preflight, launch, manage the flight operation, monitor the payload, and land the aircraft. Two flight operations are supported, nomadic flight using Follow me, and static operations for profiling missions. Additionally, this system publishes data to the cloud-based IRISS Live situational awareness system, in the background.

To support Follow Me operations, the NNC derives guidance commands for the aircraft based on the relative position and velocity between the aircraft and the Tracker, to have the aircraft follow the Tracker (Figure 6). An operator in the Tracker being followed is able to provide offsets to the aircraft in a Tracker-relative frame, for example, the aircraft can be commanded to follow a point 100 m in front and 200 m to the left of the location and velocity of the Tracker. This feature allows the Visual Observer to place the aircraft in the best location to observe it as well as to increase safety, for example, to be placed on the opposite side of the road from power lines or trees. The NNC commands the airspeed of the aircraft, and also

derives and reports the ground speed of the aircraft so that the Tracker can adjust its speed to match. The RAAVEN is most efficient flying at an airspeed of approximately 18 m/s, however, large wind velocities can lead to highly variable ground speeds. As a result, the NNC also provides a "slaloming mode" whereby the aircraft follows a zig-zag pattern such that the average speed along the ground is reduced compared to the airspeed. Finally, the NNC continually updates the Return-to-Launch reference location in the RAAVEN's autopilot to be the location of the Tracker. The Return-to-Launch location is where the aircraft goes and loiters if it ever loses communication with the ground station.

For static profiling operations, the NNC system uses an altitude controller to enable automated relative altitude profiling. The operator is able to control the floor, ceiling, and ascend/descent rate. Given that the altitude controller is independent of the Follow Me controller, both modes can be used in parallel, to profile in nomadic applications.

#### 3.6 | Coordination interface

The customized *IRISS Live* operator interface was designed for dispersed operations of multiple aircraft simultaneously. It provides a map display with weather data, position information for all aircraft and ground support vehicles, and chat features that allow an aircraft operations manager to coordinate airspace in satisfaction of all Federal Aviation Administration regulations for nomadic UAS operation. The NNC connects locally to *IRISS Live* while also sending data to a web server through cellular service to the public Internet. This server then feeds live data through a web interface provided to collaborators and mission participants. The Mission Planner interface is an open-source software package for commanding the ArduPilot autopilot. It is used for some basic preflight procedures and as a back-up during flight operations.

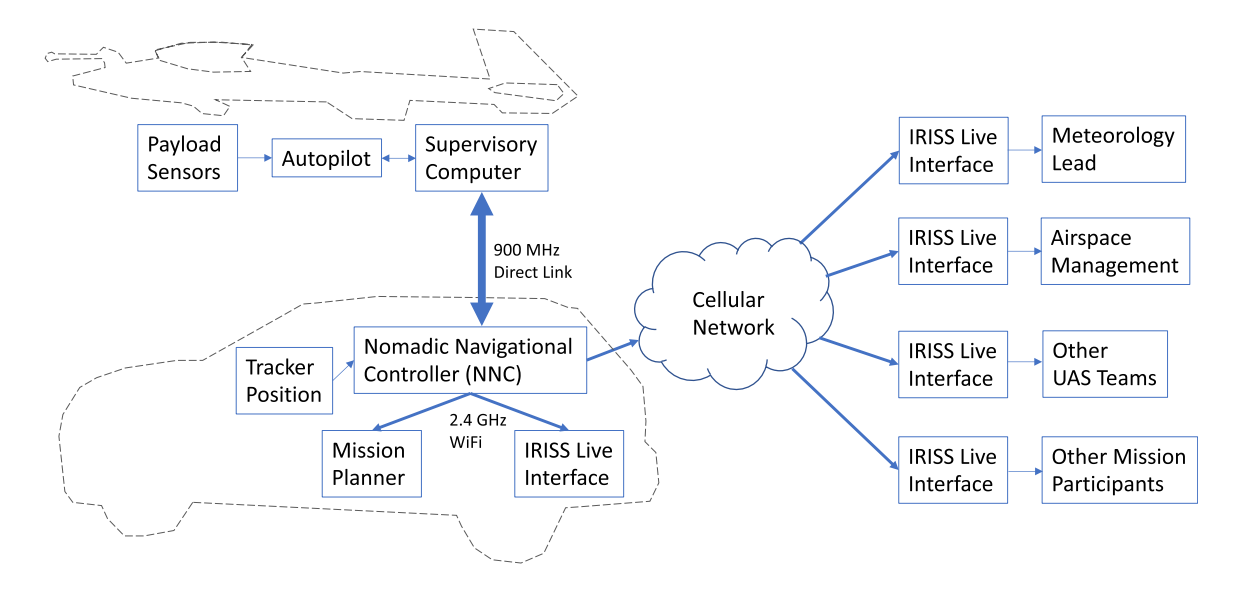


**FIGURE 5** Autonomy architecture for nomadic operation of the RAAVEN system and Tracker vehicle using the Follow Me capability [Color figure can be viewed at wileyonlinelibrary.com]

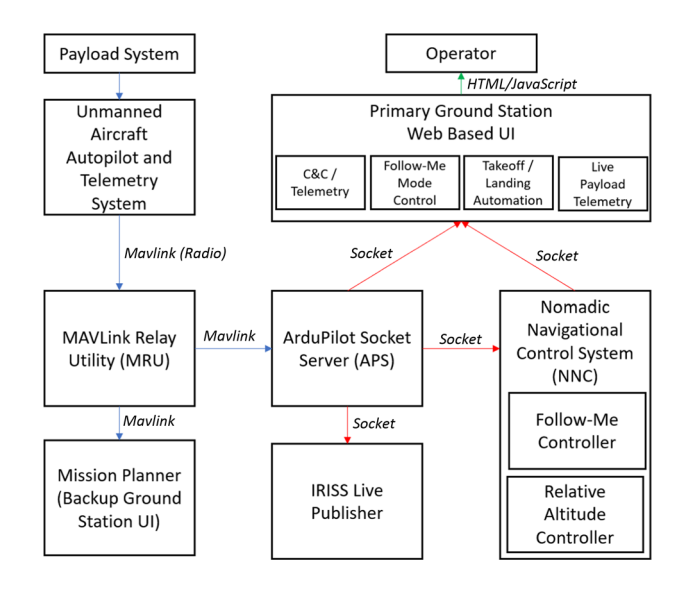


**FIGURE 6** Schematic diagram of the components of RAAVEN unmanned aircraft system that interact with the Nomadic Navigational Controller to enable the Follow Me behaviors [Color figure can be viewed at wileyonlinelibrary.com]

#### 4 | FIELD CAMPAIGN

This section describes results obtained from missions over the first 4 days of the TORUS 2019 campaign on May 17, 2019–May 20, 2019. A *mission* refers to the coordinated deployment of the instruments of the entire TORUS armada on a single storm. A single day may have more than one mission. Within a mission, the UAS team deploys multiple *aircraft* which may conduct multiple *flights*.

Table 1 summarizes the date, time, and key features of the missions. They took place in Nebraska, then Oklahoma, and finally Texas, demonstrating the scope of the nomadic activities associated with this type of field campaign. The launch time is included to show that flights occur in the late afternoon or early evening, and that the COA limitations can impact the mission. Note, all times are reported as Central Daylight Time. Due to aircraft issues and logistical limitations, not every team flew every mission. The final column in Table 1 indicates whether the storm was tornadic, meaning it produced at least one tornado at some point before, during, or after flight in that storm.

The summaries of all four missions are presented below. The first mission on May 17, 2019 is discussed in greater detail to demonstrate the full concept of operation relative to the supercell

thunderstorm. The other missions followed similar patterns and are not described in as much depth, though new or unique aspects of these missions are highlighted.

# 4.1 | Mission 1 May 17, 2019

The first operational deployment of TORUS 2019 was conducted on May 17, 2019 where the left flank, right flank, and near inflow aircraft were deployed on a tornadic (Figure 1) supercell near Lexington, NE. The National Weather Service (NWS) Goodland and North Platte services recorded a total of eight tornadoes, golf-ball-size hail and winds exceeding 50 mph (NWS, 2019) from this storm. Figure 7 shows views of the target storm from the perspective of the rear flank team.

The top of Figure 8 shows the complete flight path of the left flank and right flank aircraft, as well as the two different, loiter locations for the near inflow team. The storm itself is not included on this plot for since it moves over the duration of the mission, and to allow for a clear presentation of the flight paths. The bottom of Figure 8 shows the height of each aircraft versus time. Combined, these plots show the spatial extent of the aircraft flights and how they were coordinated in time.

The path of each aircraft can be seen in relation to the target storm in Figure 9. The figure includes snapshots at 10 min increments (labeled above the subfigures) of the National Weather Service WSR-88D "NEXRAD" radar composite reflectivity along with the aircraft paths from launch to that moment in time. In the target storm, the left flank was positioned to the northeast of the hook echo and the right flank formed to the southeast. The LF, RF, and NI teams all deployed (Figure 9a) on the supercell that was moving to the northeast. The LF aircraft was the first to takeoff to the northeast of the storm center. The NI aircraft followed a few minutes later and began profiling maneuvers. It performed two profiles (Figure 9b) and landed. Finally, the RF aircraft took off and initially flew north toward the supercell. As the front of the storm passed over, the NI aircraft took off again to perform a second profiling mission (Figure 9c). After 10 min the NI aircraft landed and repositioned to the east of the moving storm (Figure 9g). The first transect of the LF aircraft sampled a region of the storm with high amounts of precipitation (Figure 9a-c). The LF aircraft then descended and backtracked east to complete the full transect (Figure 9d-f). After completing the transect, the LF team moved

**TABLE 1** Unmanned aircraft system missions

Mission number	Date	Approx. launch time	Nearest town	Teams	Tornadic
1	May 17, 2019	18:15 CDT	Cambridge, NE	LF, RF, NI	Υ
2	May 18, 2019	18:13 CDT	Cherokee, OK	LF, RF	N
3	May 20, 2019	15:51 CDT	McQueen, OK	LF, RF, NI	Υ
4	May 20, 2019	19:48 CDT	Crowell, TX	Stack	N

Abbreviations: LF, left flank; NI, near inflow; RF, right flank.





**FIGURE 7** The left image shows the Tracker and CoMeT vehicles for the right flank team in front of the target storm. The right image shows the RF aircraft (within red circle) and the P3 aircraft (blue circle) in front of the target storm of Mission 1 [Color figure can be viewed at wileyonlinelibrary.com]

north to match the movement of the storm and remained in the region of the left flank (Figure 9f–i). After launch, the RF aircraft continued to move north towards the storm (Figure 9a–d). Approximately 30 min into flight, communication performance degraded between the RF aircraft and tracker vehicle. Therefore, the RF aircraft remained stationary from this point and performed vertical profiles as the storm moved past (Figure 9e–i).

Air temperature (C°), air pressure (mbar), and relative humidity (%) values recorded by each aircraft for the May 17, 2019 storm are shown in Figure 10. These values demonstrate the ability of the aircraft to measure important thermodynamic quantities from different regions of the supercell simultaneously. Pressure values appear to track with the altitude of the aircraft. The relative humidity of the LF aircraft (third plot of Figure 10) indicates that initially, the LF aircraft flew into a region of high relative humidity, as also seen in the radar reflectivity in Figure 9b-c. The precipitation-heavy portion of the storm then begins to move northwards, away from the LF aircraft (Figure 9d). In the relative humidity plot in Figure 10 values for the LF, aircraft dip and level off for 15 min during this period. As the LF aircraft moved back toward the precipitation region at the core of the storm, that relative humidity value rises again. For the same storm, the RF measured an increase in relative humidity 15 min into the flight. The values then oscillated as the aircraft performed profiles, indicating that the relative humidity was higher at higher altitudes in the rear-flank gust in front of the storm.

Features of the storm morphology can be observed or inferred from the data in Figures 8, 9, and 10. For example, the altitude drop in Figure 8 with the corresponding pressure increase in Figure 10 just after 18:30 indicates a downward shift in aircraft height, likely due to a downdraft. Another example is that the relative humidity tracks with altitude in the LF and RF, indicating more moisture aloft in both parts of the storm, although for the LF, the relative humidity is initially decreasing and temperature increasing during the climb, until 18:15, a reverse trend that suggests a boundary-crossing.

# 4.2 | Mission 2 May 18, 2019

On May 18, 2019 a nontornadic supercell near Cherokee, OK was intercepted (Figure 11). The RF and LF teams successfully deployed their aircraft (Figure 12). Both aircraft performed transects of their target regions. The LF aircraft stepped down in altitude (from time 18:35 to 18:40) to measure the left-flank at different altitudes. Due to a faulty initial launch, the NI mission was unable to perform the profiling mission. After this, the pilot in command chose not to attempt a relaunch and the team was grounded for the day.

Compared to Mission 1, these flights were mostly straight with fewer zig-zags or orbits. These maneuvers are induced when the Tracker vehicle drives too slow and the aircraft has to reduce its ground speed to keep up. This mission also shows how the overall sampling performance is tied to the road network, as both aircraft make several obvious 90-degree turns that correspond to the Tracker turning on to different roads. Further, the two aircraft end the mission on the same road, even though they are trying to sample different regions of the storm. In this case, the storm motion changed relative to its path when the aircraft were initially positioned, and there were a limited number of roads the Tracker vehicles could use.

# 4.3 | Mission 3 May 20, 2019

The third supercell on May 20, 2019 in the vicinity of McQueen, OK was intercepted by the RF, LF, and NI teams (Figure 13). The National Weather Service Storm Prediction Center issued a high-risk warning for severe weather events over much of the U.S. Great Plains on that day. This warning received extra attention on news broadcasts and made the UAS teams especially attentive to the potential for other traffic on the road networks the Trackers would use. The UAS teams also knew there could be multiple storms over the day and prepared to conduct multiple missions by carrying multiple charged battery packs for each aircraft.

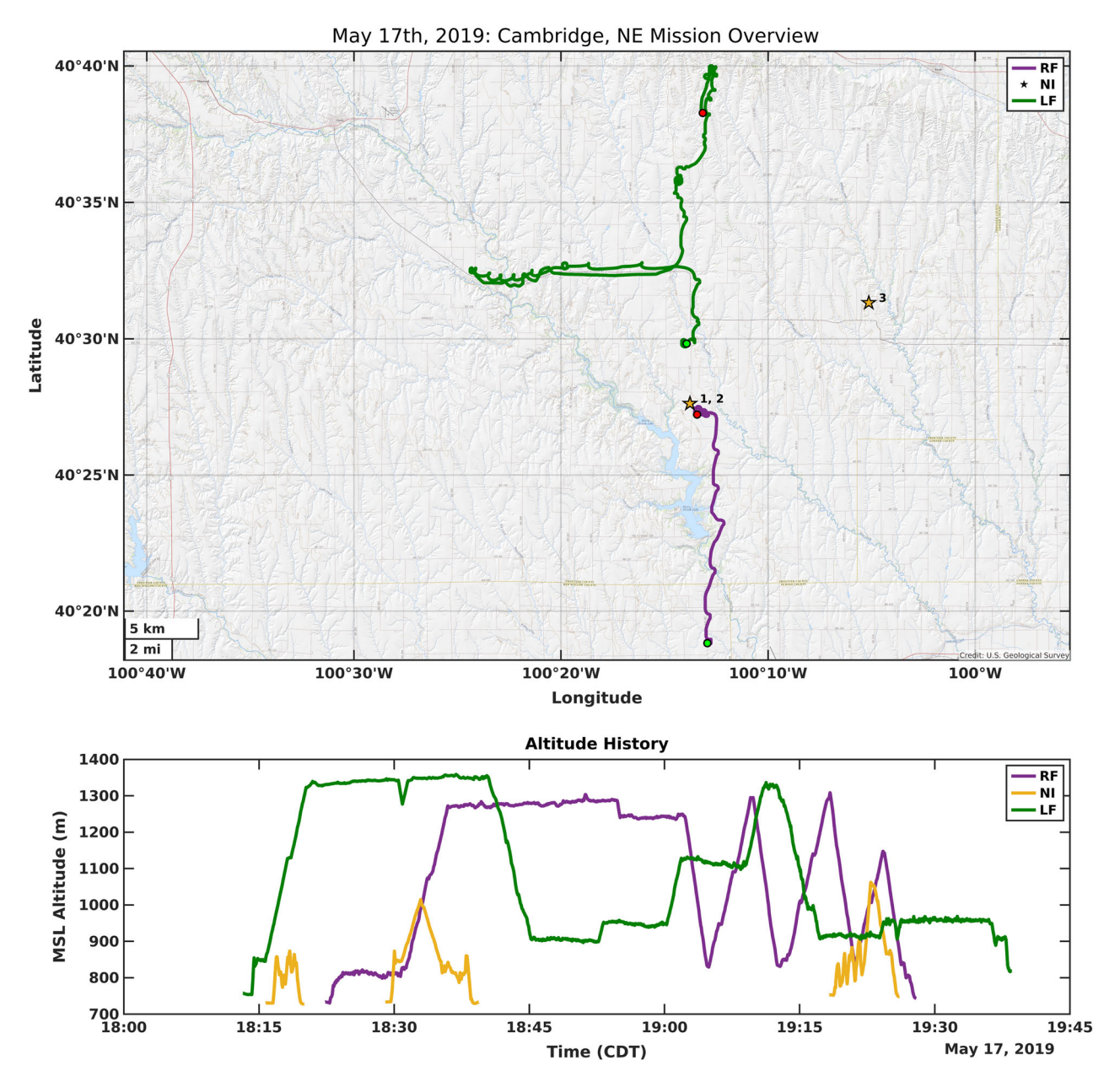


**FIGURE 8** Flight history for May 17, 2019 mission. The top plot shows the flight path of the LF (green) and RF (purple) aircraft, as well as the two different loiter locations for the NI (gold) team. The green circles indicate the location of launch, while the red indicates where the aircraft landed. The star is used when the aircraft loiters and the launch and land locations are indistinguishable. The bottom plot shows the altitude of each aircraft versus time. Gaps in the lines indicate the aircraft was on the ground and/or was moving to a new location. LF, left flank; NI, near inflow; RF, right flank [Color figure can be viewed at wileyonlinelibrary.com]

The RF and LF aircraft performed successful transects of their respective storm regions while the NI aircraft profiled for approximately 50 min. The LF and RF teams flew at a variety of discrete altitudes to sample multiple portions of their respective flanks. Like Mission 1, the LF aircraft was able to fly east into the left flank and orbit in this region. The RF aircraft spent more time moving north to enter the storm. The wavy paths suggest the aircraft was flying in a tailwind and needed to reduce speed relative to the Tracker which was not able to drive fast enough to keep up with it. The profiling behavior of the NI aircraft is especially clear in the altitude plot in Figure 13. The measured

altitude oscillates over the 50 min window of the flight as the aircraft performs vertical profiles.

This mission also highlights the challenges in finding safe landing spots for the aircraft. After the LF team samples the storm (as shown by the orbits at the western edge of the flight path in Figure 13), it travels straight east for a long stretch before turning north and landing. During this time the LF team is outracing the storm to gain enough time to land without being exposed to heavy rain, hail, or lightning. In contrast, the RF team finishes its mission and lands at the same location where the LF team was in the storm. This occurs

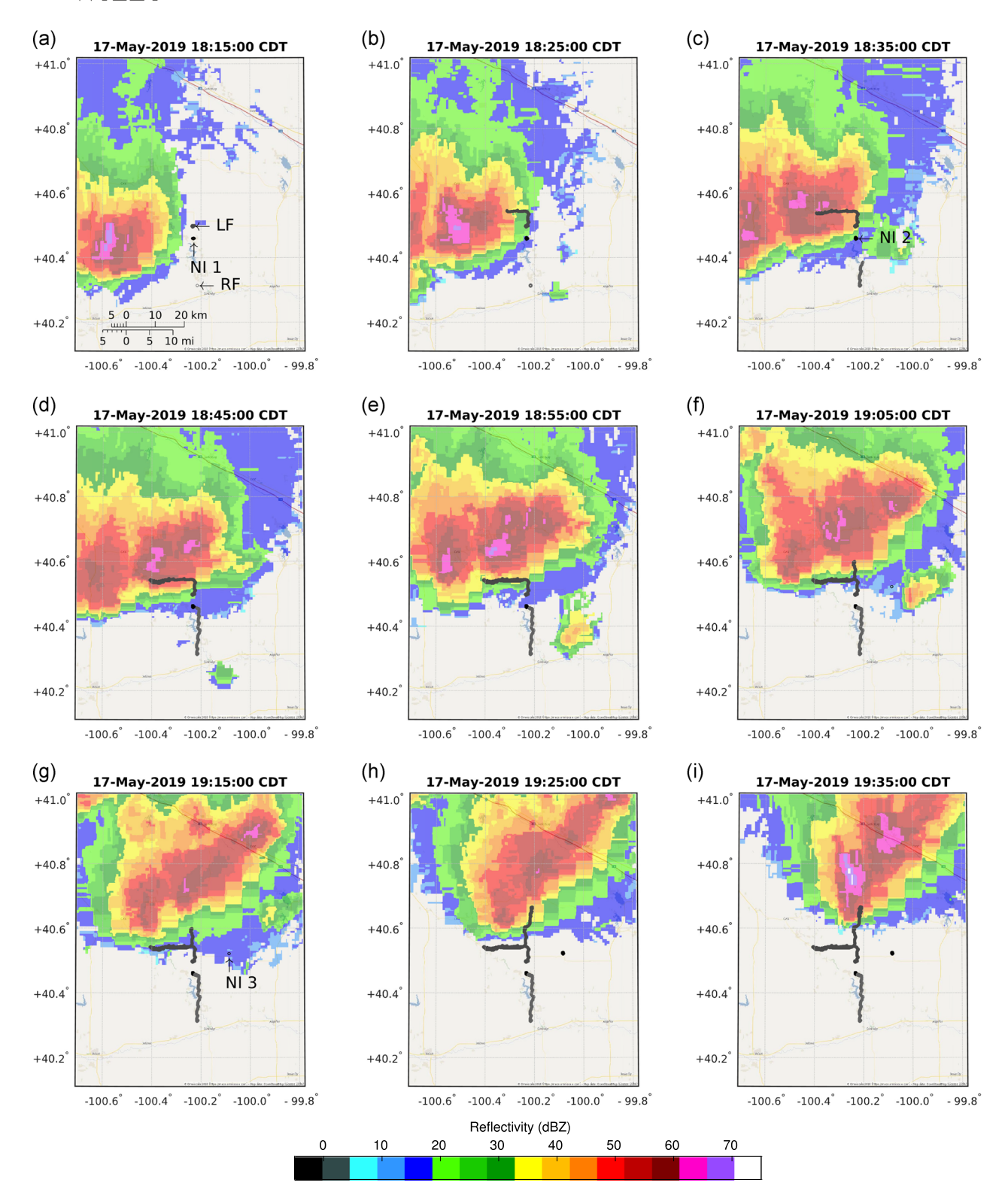
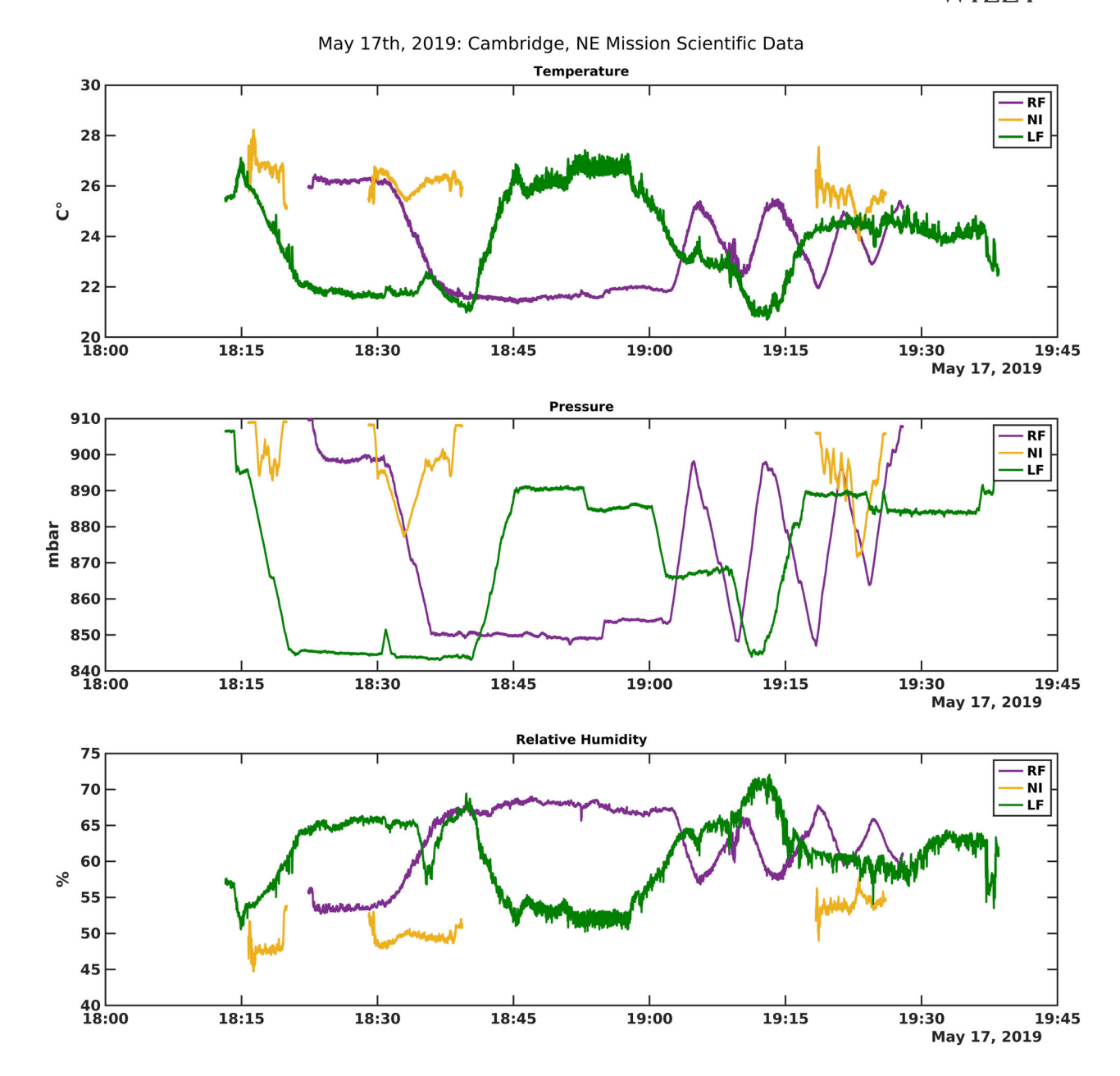


FIGURE 9 WSR-88D "NEXRAD" radar composite reflectivity for May 17, 2019 along with the aircraft flight paths from launch until that moment. Date and time for each snapshot are included above the subfigure. The aircraft team is labeled in the subfigure when the aircraft flight first appears. The LF and RF aircraft are flying the entire time while the NI aircraft has three different flights. The colorbar at the bottom indicates the values of the radar reflectivity. Higher reflectivity correlates with more precipitation. LF, left flank; NI, near inflow; RF, right flank [Color figure can be viewed at wileyonlinelibrary.com]



**FIGURE 10** Temperature (C°), pressure (mbar), and relative humidity (%) values vs. time recorded by each aircraft for the May 17, 2019 mission [Color figure can be viewed at wileyonlinelibrary.com]



**FIGURE 11** The target storm for Mission 2 as viewed from the near inflow region [Color figure can be viewed at wileyonlinelibrary.com]

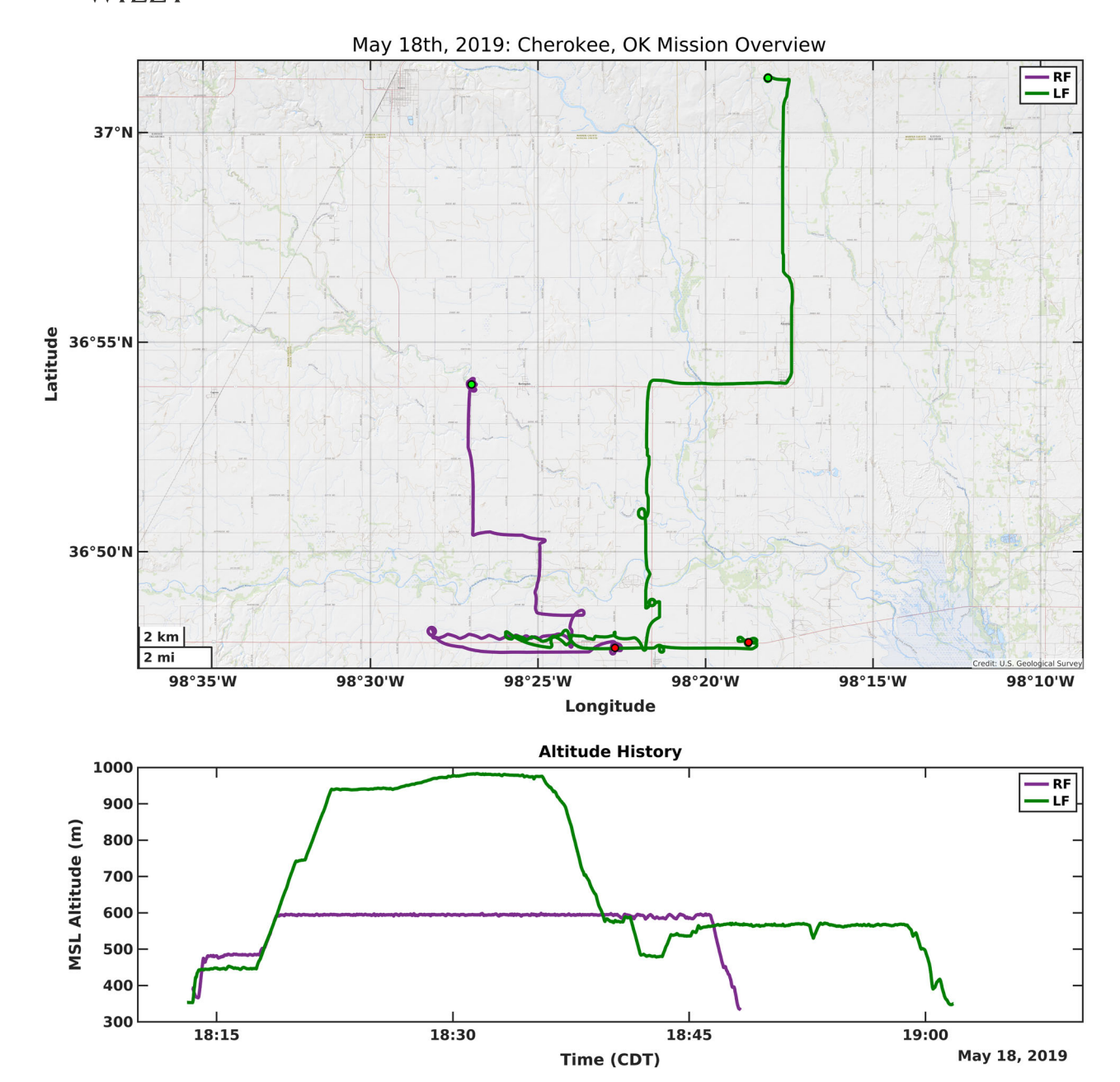


**FIGURE 12** Flight history for May 18, 2019 mission. The top plot shows the flight path of the LF (green) and RF (purple) aircraft. The green circles indicate the location of launch, while the red indicates where the aircraft landed. The bottom plot shows the altitude of each aircraft vs time. LF, left flank; RF, right flank [Color figure can be viewed at wileyonlinelibrary.com]

because the RF team travels from beneath the storm and into the rear-flank region as the storm passes. This region is free of precipitation and safe for landing by the time the RF team arrives.

#### 4.4 | Mission 4 May 20, 2019

The second mission on May 20, 2019 (Mission 4) near Crowell, TX (Figure 14) made use of a stack configuration using the RF and LF aircraft. After Mission 3, the entire TORUS team took approximately 2 hours (from 17:30 CDT to 19:30 CDT) to reposition relative to a

new target storm. During this time the NI team's ground vehicles became inoperable and the NI aircraft did not redeploy. Due to limitations of the road network, the storm motion, and decreasing visibility, the RF team was not likely to take its position in time and the decision was made to fly both aircraft in the stack configuration in the LF team's region of the storm. The two aircraft were positioned such that one aircraft flew above the other with a vertical separation distance of approximately 200 m, shown in Figure 15. The two aircraft then performed horizontal transects of the storm. A rapid power drop on the RF aircraft caused this mission to end after approximately 20 min.

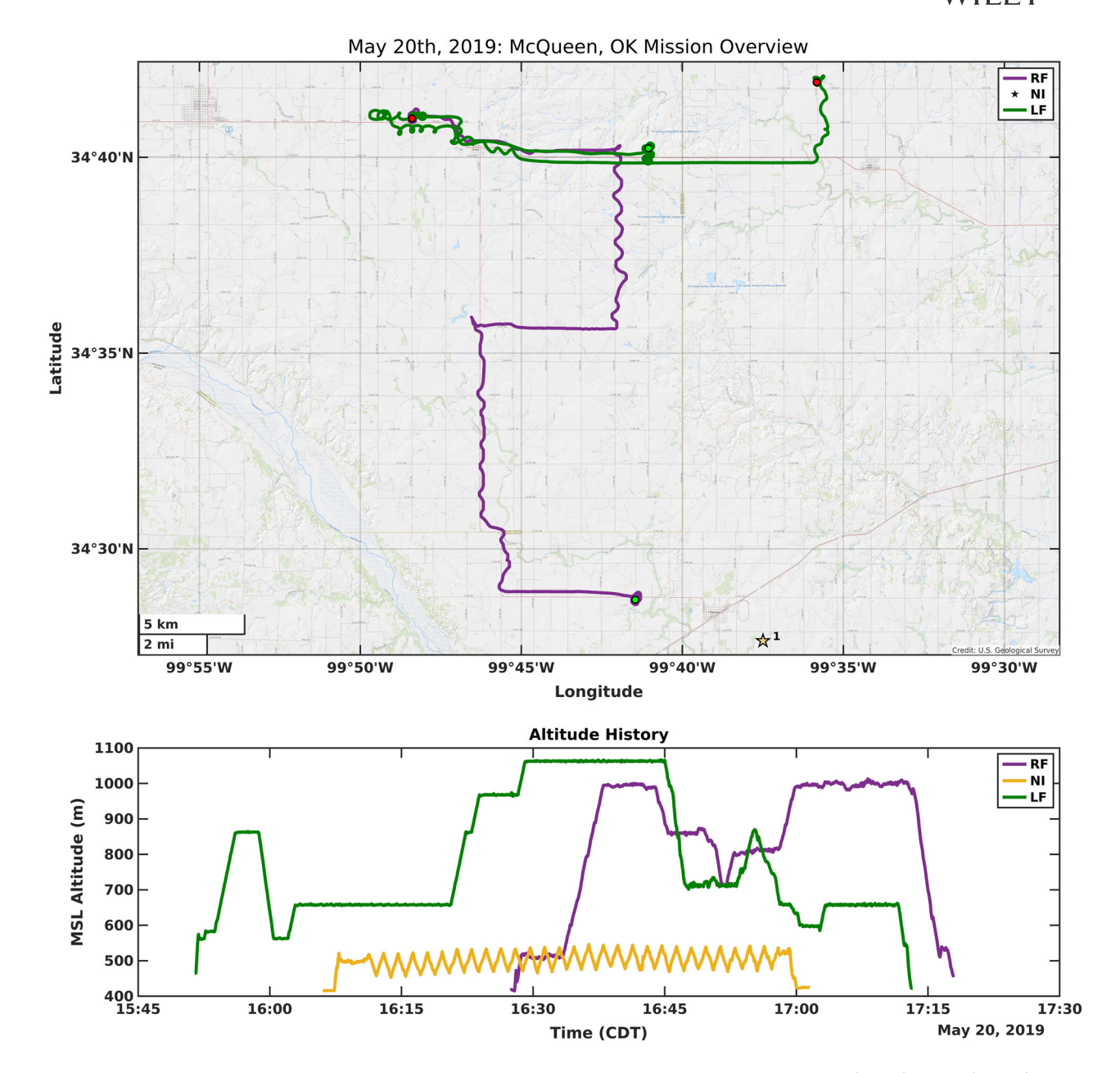


FIGURE 13 Flight history for the first May 20, 2019 mission. The top plot shows the flight path of the LF (green) and RF (purple) aircraft, as well as the loiter location for the NI (gold) team. The green circles indicate the location of launch, while the red indicates where the aircraft landed. The bottom plot shows the altitude of each aircraft vs. time. LF, left flank; NI, near inflow; RF, right flank [Color figure can be viewed at wileyonlinelibrary.com]

Mission 4 is notable for two reasons. First, this was the first time the UAS team deployed on multiple storms in a single day. As noted for Mission 3, the weather forecast called for multiple storms throughout the day and night, so the UAS team ensured that extra batteries were charged and extra equipment was available for fast repair in the field. The process from ending Mission 3, collecting the aircraft, and repositioning for Mission 4 was rapid and demonstrated the value of the RAAVEN design not just for quick launch, but for ease of use in general. Second, this mission was the first time the stack configuration was used. During the stack flight, the LF and RF aircraft followed their own respective Tracker vehicles, but only a single CoMeT vehicle led the team.

#### 5 | DISCUSSION

Successful field deployment of multiple unmanned aircraft studying supercell thunderstorms can be attributed to (a) a professional crew with over 10 years experience developing and deploying UAS in severe weather, (b) a nomadic concept



FIGURE 14 The left image shows the target storm for Mission 4 from afar, approximately one hour before flight. The right image shows conditions of the target storm when landing the aircraft [Color figure can be viewed at wileyonlinelibrary.com]

of operations that allows the UAS team and science team to work seamlessly together while satisfying all aviation regulations, and (c) a ruggedized unmanned aircraft system with modular features that favor rapid ease of use over the strength of previous designs (Elston, Roadman, et al., 2011). Crew experience and training is beyond the scope of this paper, so lessons learned for the concept of operations, UAS design, and the interplay between them are shared below.

The importance of the RAAVEN's durability and ease of use cannot be overstated. Every instrument onboard the aircraft worked almost all of the time, enabling consistent deployment. The modularity of the physical elements of the RAAVEN platform, electronics, and payload sensors was also critical—the UAS team was able to repair aircraft quickly and could even take parts from one aircraft and use them on another. This modularity was especially helpful since the aircraft supervisory computers were hard-coded to interface with a specific Tracker vehicle.

Fast, reliable launch and landing were critical to mission success. The RAAVEN design chose to sacrifice some strength in the aircraft platform (compared to previous generation aircraft Roadman et al., 2012) in return for easier, faster deployment. The guiding design philosophy was that mission success was more likely with many quicker deployments compared to fewer deployments with a stronger aircraft. Faster deployment time meant the UAS teams could get closer to the storms and regions of interest before deployment. Thus less flight time was spent ingressing and more flight time was spent gathering science data. As noted for Mission 4, being able to rapidly land and disassemble the aircraft was also important to enable multiple missions in a single day. Knowing the UAS could fly more than once, the science leads could be more aggressive in choosing to study marginal storms early in the day rather than waiting for the one "best" case.

The nomadic operations described here had the visual observer and pilot in command in the Tracker vehicle collocated with the aircraft. By having the pilot in command close to the aircraft, the direct 900 MHz communication link from the Tracker to the aircraft only had to cover a few miles (the worst case separation distance). This specification simplified the design of the communication system compared to previous systems where the pilot in command was in a stationary ground control station up to 20 miles away from the aircraft (Elston, Roadman, et al., 2011).

A useful feature of the nomadic navigational controller was the ability of the operator to issue offsets for the aircraft path relative to the Tracker. During flight, the avionics system worked well and the operator only used telemetry from the autopilot to determine the remaining flight time from the battery state. The operator's main task was commanding offsets of the aircraft to account for terrain, radio towers, upcoming turns in the road, and so forth. The ability to issue these offsets increased the efficiency of the aircraft (e.g., by cutting turns and reducing loiters) and safety (e.g., by switching to the side of the Tracker away from power lines or to give the visual observer a better view of the aircraft).

Coordination across the LF, RF, and NI teams was critical for smooth operation. IRISS Live was the backbone for communication within the UAS team. Because IRISS Live was written as a web interface to a server maintained by the UAS team, it was straightforward to add functionality in the field. Over the initial missions the UAS team determined that additional features needed to be implemented. These features included a chat interface, tracking, and displaying all unmanned aircraft and the participating P3 aircraft, visualization of areas/hazards to avoid, and interface to request and move the NOTAMs issued to the Federal Aviation Administration to designate areas of operation. The IRISS Live interface was a success in part because cellular connectivity was available throughout the domain of operation. Anecdotally, the coverage was much better than during the

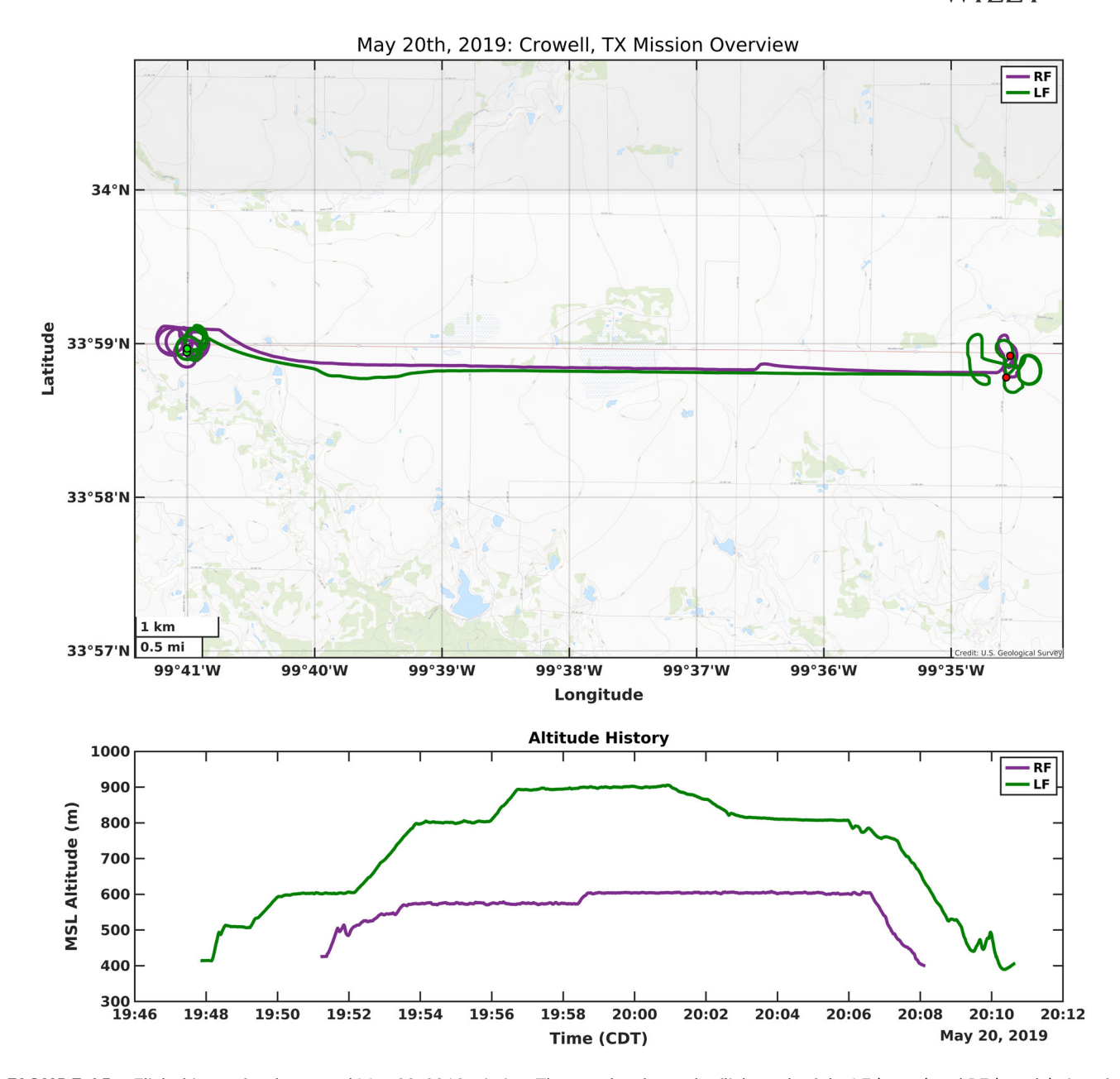


**FIGURE 15** Flight history for the second May 20, 2019 mission. The top plot shows the flight path of the LF (green) and RF (purple) aircraft. The green circles indicate the location of launch, while the red indicates where the aircraft landed. The bottom plot shows the altitude of each aircraft vs. time. LF, left flank, RF, right flank [Color figure can be viewed at wileyonlinelibrary.com]

VORTEX2 campaign (Elston, Roadman, et al., 2011) and coordination was much easier than expected.

Since the purpose of the UAS flights was collecting data to study the supercell thunderstorms, a smooth workflow for handling all telemetry and payload measurements is important. Most of the preflight and immediate postlaunch tasks involved confirming that payload sensors are recording data. Because payload data is sent to the ground station at a low data rate, the operation can be verified before the Tracker starts traveling down the road for the main portion of the mission. After the flight, data is located on an SD card on the aircraft. Because this data is

overwritten with each flight, the card was removed as part of the landing process. These cards are labeled and stored, with a new card used for every mission. Data processing scripts were created in advance and run at the end of the day once the operation was completed. Verifying system performance by looking at processed results was helpful, but did not play a significant role in mission planning for the following day since a full understanding of the meaning of the data will not occur until all data sets from all TORUS instruments are analyzed together.

A full understanding of the significance of the data collected during these flights will only occur in the context of the entire 2-year

field campaign. The UAS data will be combined with data from the other TORUS instruments (mobile radars, airborne radar, lidar, weather balloons, and mobile mesonets) to address the hypotheses posed. The results presented here show the unique (i.e., spatially distributed, simultaneous, in situ) measurements enabled by multiple coordinated unmanned aircraft

#### 6 | CONCLUSION

This paper presented results from the deployment of multiple autonomous unmanned aircraft systems during the 2019 TORUS field campaign. The concept of operations over the month-long campaign was described, along with the RAAVEN unmanned aircraft system used to study tornadogenesis through coordinated, synchronous flights of multiple aircraft in various parts of supercell thunderstorms. The system architecture of the RAAVEN was shown in detail, including the autonomy framework and scientific payload. Flight results from several missions during the first 4 days of the TORUS campaign (May 17, 2019–May 20, 2019) were presented. This study demonstrated the viability of reliably deploying multiple autonomous fixed-wind aerial robots to conduct coordinated scientific data gathering missions in extreme conditions.

#### **ACKNOWLEDGMENTS**

This study was supported by the National Science Foundation by grant AGS-1824609. Thanks to the University of Colorado Boulder Integrated Remote and In Situ Sensing (IRISS) program. Additional thanks to the entire IRISS team that deployed during TORUS 2019 which includes Anders Olsen, Aiden Sesnic, Chris Choate, Cole Kenney, Dan Hesselius, Danny Leibert, Dishank Kathuria, Dominic Dougherty, and Michael Rhodes.

#### **REFERENCES**

- Beck, J., & Weiss, C. (2013). An assessment of low-level baroclinity and vorticity within a simulated supercell. Monthly Weather Review, 141(2), 649–669.
- Bonin, T., Chilson, P., Zielke, B., & Fedorovich, E. (2012). Observations of the early evening boundary-layer transition using a small unmanned aerial system. *Boundary-Layer Meteorology*, 146(1), 119–132.
- Curry, J. A., Maslanik, J., Holland, G., & Pinto, J. (2004). Applications of aerosondes in the arctic. Bulletin of the American Meteorological Society, 85(12), 1855–1861.
- Dahl, J. M. L., Parker, M. D., & Wicker, L. J. (2012). Uncertainties in trajectory calculations within near-surface mesocyclones of simulated supercells. Monthly Weather Review, 140(9), 2959–2966.
- Dias, N. L., Gonçalves, J. E., Freire, L. S., Hasegawa, T., & Malheiros, A. L. (2012). Obtaining potential virtual temperature profiles, entrainment fluxes, and spectra from mini unmanned aerial vehicle data. *Boundary-Layer Meteorology*, 145(1), 93–111.
- Elston, J., Argrow, B., Frew, E. W., Houston, A., & Straka, J. (2011). Evaluation of unmanned aircraft systems for severe storm sampling using hardware-in-the-loop simulations. *AIAA Journal of Aerospace Computing, Information, and Communication*, 8(9), 269-294.

- Elston, J. S., Roadman, J., Stachura, M., Argrow, B., Houston, A., & Frew, E. W. (2011). The tempest unmanned aircraft system for in situ observations of tornadic supercells: Design and vortex2 flight results. *Journal of Field Robotics*, 28(4), 461–483.
- FAA. (2008). UAS certifications and authorizations. Retrieved from http://www.faa.gov/aircraft/air\_cert/design\_approvals/uas/cert/
- FAA. (2019). Certificated remote pilots including commercial operators. Retrieved from https://www.faa.gov/uas/commercial\_operators/
- Frew, E. W., Elston, J., Argrow, B., Houston, A., & Rasmussen, E. (2012). Sampling severe local storms and related phenomena: Using unmanned aircraft systems. *Robotics and Automation Magazine*, 19(1), 85–95.
- Hanft, W., & Houston, A. L. (2018). An observational and modeling study of mesoscale air masses with high theta-e. Monthly Weather Review, 146, 2503–2524.
- Holland, G. J., Webster, P. J., Curry, J. A., Tyrell, G., Gauntlett, D., Brett, G., & Vaglienti, W. (2001). The aerosonde robotic aircraft: A new paradigm for environmental observations. Bulletin of the American Meteorological Society, 82(5), 889-901.
- Jacob, J. D., Chilson, P. B., Houston, A. L., & Smith, S. W. (2018). Considerations for atmospheric measurements with small unmanned aircraft systems. Atmosphere, 9(7), 7.
- Kosiba, K., Wurman, J., Richardson, Y., Markowski, P., Robinson, P., & Marquis, J. (2013). Genesis of the Goshen County, Wyoming, tornado on 5 June 2009 during VORTEX2. Monthly Weather Review, 141(4), 1157–1181.
- Lemon, L. R., & Doswell, C. A. (1979). Severe thunderstorm evolution and mesocyclone structure as related to tornadogenesis. Monthly Weather Review, 107(9), 1184–1197.
- Lin, P.-H., & Lee, C.-S. (2008). The eyewall-penetration reconnaissance observation of typhoon longwang (2005) with unmanned aerial vehicle, aerosonde. *Journal of Atmospheric and Oceanic Technology*, 25(1), 15–25.
- Nichols, T., Argrow, B., & Kingston, D. (2017). Error sensitivity analysis of small UAS wind-sensing systems. In AIAA Infotech at Aerospace.
- NWS. (2019). May 17, 2019, tornadoes and severe weather—updated. Retrieved from https://www.weather.gov/lbf/tornadoes17may2019
- Orf, L., Wilhelmson, R., Lee, B., Finley, C., & Houston, A. (2017). Evolution of a long-track violent tornado within a simulated supercell. *Bulletin of* the American Meteorological Society, 98(1), 45–68.
- Reuder, J., Brisset, P., Jonassen, M., Müller, M., & Mayer, S. (2009). The small unmanned meteorological observer SUMO: A new tool for atmospheric boundary layer research. *Meteorologische Zeitschrift*, 18, 141–147.
- Roadman, J., Elston, J., Argrow, B., & Frew, E. W. (2012). Mission performance of the tempest uas in supercell storms. AIAA Journal of Aircraft, 49(6), 1821–1830.
- Sand, W. R. (1976). Observations in hailstorms using the T-28 aircraft system. *Journal of Applied Meteorology*, *15*(6), 641–650.
- Skinner, P. S., Weiss, C. C., French, M. M., Bluestein, H. B., Markowski, P. M., & Richardson, Y. P. (2014). VORTEX2 observations of a low-level mesocyclone with multiple internal rear-flank downdraft momentum surges in the 18 May 2010 Dumas, Texas, supercell.
- Snyder, J. C., Bluestein, H. B., Venkatesh, V., & Frasier, S. J. (2013). Observations of polarimetric signatures in supercells by an X-band mobile Doppler radar. *Monthly Weather Review*, 141(1), 3-29.
- TORUS. (2019). Targeted observation by radars and UAS of supercells. Retrieved from https://torus.unl.edu/
- van den Kroonenberg, A. C., Martin, S., Beyrich, F., & Bange, J. (2012). Spatially-averaged temperature structure parameter over a heterogeneous surface measured by an unmanned aerial vehicle. Boundary-Layer Meteorology, 142(1), 55–77.
- VORTEX2. (2008). Vortex2. Retrieved from http://www.vortex2.org/

# SUPPORTING INFORMATION

Additional supporting information may be found online in the Supporting Information section.

**How to cite this article:** Frew EW, Argrow B, Borenstein S, et al. Field observation of tornadic supercells by multiple autonomous fixed-wing unmanned aircraft.

J Field Robotics. 2020;1–17.

https://doi.org/10.1002/rob.21947

# APPENDIX: INDEX TO MULTIMEDIA EXTENSIONS

The following table describes the video included in the online version of this article.

Extension	Media type	Description
1	Video	Operation of the RAAVEN unmanned aircraft system during the TORUS field campaign, including launch, sampling, and landing along with onboard footage of several storms.